Research Article | Vol. 27, No. 13 | 24 Jun 2019 | OPTICS EXPRESS 18399
Optics EXPRESS

Broad visible spectral subwavelength polarizer with high extinction ratio using hyperbolic metamaterial

WEI ZHANG, XIN TAN, NA WU, WENHAO LI,* QINGBIN JIAO, AND SHUO YANG

Changchun Institute of Optics, Fine Mechanics and Physics, Chinese Academy of Sciences, No. 3888 Dong Nanhu Road, Changchun, Jilin, 130033, China
**liwh@ciomp.ac.cn*

Abstract: A subwavelength polarizer with an extinction ratio greater than 50 dB in the visible region (exceeding 80 dB in the 500 to 800 nm wavelength region) is presented that uses hyperbolic metamaterial decorated on each side with a subwavelength grating. The approach is based on the spatial frequency filtering characteristics of the hyperbolic metamaterial with its alternating metal-dielectric nano-film, which enables squeezing of bulk plasmon polaritons to support transverse magnetic polarized light transmission in the high spatial wavevector modes while suppressing other polarization mode waves over the broad visible spectrum. The proposed method exhibits a more realizable fabrication process than that used for a subwavelength polarizer based on high-aspect-ratio grating for broad spectrum and high-extinction-ratio performance. The subwavelength polarizer in this work is potential for the high-sensitivity polarimetric imaging.

1. Introduction

In optical imaging systems, control of light polarization is a crucial issue [1–3]. However, the pursuit of miniaturization and integration for modern optical systems represents a problem for bulky conventional polarizers, including prism polarizer, dichroic glass polarizer, birefringent-crystal-based polarizer and polarcor polarizer. The wire grid polarizer (WGP), which is composed of a subwavelength metal grating, exhibited excellent polarization performance in a seminal investigation for the near-infrared waveband [4]. Since then, the WGP has been shown to offer compactness, high polarization efficiency, a wide field of view, and long-term stability, and many aspects of the WGP have been studied in optical science.

The polarimetric performance of the WGP is affected by its grating period, duty cycle and aspect ratio. For WGP for use in the visible region, grating fabrication with high groove density is challenging and state-of-the-art micro- and nano-fabrication technology must be used in place of conventional single-exposure interference lithography technique, include electron beam lithography (EBL), immersion interference lithography, deep ultraviolet (DUV) and extreme ultraviolet (EUV) interference lithography, and nanoimprint lithography.

In 1997, Tamada fabricated an Al grating with 390 nm period using EBL [5]. This polarizer realized 50% transmission efficiency for the transverse magnetic (TM) polarization and extinction ratio of 1000 (30 dB) at the wavelength of 780 nm. Subsequently, nanoimprint lithography was used to fabricate Al gratings with 100 nm period and 200 nm groove depth [6], which allowed a subwavelength polarizer with extinction ratio of 2000 (33 dB) to be obtained at a wavelength λ = 450 nm. A nanoimprint stamp was fabricated by laser interference lithography and spatial frequency doubling technique. To enable further improvement in the WGP performance, two 190-nm-period Au grating layers with depth of 70 nm were fabricated by nanoimprint lithography [7] and a polarizer was realized with extinction ratio of 225 (23.5 dB) for the 632.8 nm wavelength.

#364304 https://doi.org/10.1364/OE.27.018399
Journal © 2019 Received 8 Apr 2019; revised 11 May 2019; accepted 19 May 2019; published 17 Jun 2019

Optics EXPRESS

Furthermore, some subwavelength polarizers have been proposed for operation in the visible spectral band. In 2006, Al nanowire gratings were fabricated on both sides of a glass wafer with 149 nm period and depth of 200 nm using UV-nanoimprint lithography [8]. The extinction ratio of this structure was more than 2500 (34 dB) within the wavelength range from 450 nm to 700 nm. Swiss researchers used EUV interference lithography to fabricate a stacked Al grating with 100 nm period and 94 nm depth difference [9]. The extinction ratio of their polarizer reached 1000 (30 dB) in the visible region from 400 nm to 800 nm. Another subwavelength polarizer with wire grids in a tandem configuration was also simulated theoretically and exhibited higher extinction ratio. In 2012, an MgF_2 film was added between the glass substrate and the wire grid grating [10], and this structure realized the extinction ratio of 370 (25.7 dB) in case of a grating with 200 nm period and depth of 175nm over the wavelength range from 380 nm to 520 nm.

However, for a WGP with higher extinction ratio, grating with smaller period and higher aspect ratio is needed. Additionally, for the blue light region, the period of the metal grating is required to reach the deep subwavelength level [11]. While the unconventional methods described above can provide sufficient resolution, they also have some very obvious disadvantages. The throughput of EBL is very low. Liquid immersion interference lithography offers only a limited field size and requires high-precision process control. DUV or EUV interference lithography technique requires high-cost light source and some high-quality optical lenses. Nanoimprint lithography offers the advantages of low cost and high throughput processing, but the stamp fabrication procedure is complex and expensive [12]. Therefore, WGP with higher extinction ratio requires mounting of metal patterns with larger aspect ratio, which involves more difficult lithographic techniques and leads to more complex fabrication processes.

Recently, subwavelength polarizer based on surface plasmon resonance was designed theoretically and achieved high extinction ratio but exhibited narrowband characteristic [13–16]. Peltzer proposed the use of a pair of dielectric-coated metal gratings with a central subwavelength aperture to act as a metal-insulator-metal (MIM) waveguide, which enable incident TM-polarized light to be coupled into surface plasmon and thus be transported through the central aperture. Extinction ratio exceeding 1011 (30 dB) was predicted via simulation for the wavelength of 635 nm [15]. To obtain improved polarimetric performance, a plasmon-enhanced WGP with a blazed profile grating was proposed [16] and its extinction ratio reached 42 dB at a wavelength of 800 nm.

At present, a high-extinction-ratio polarizer is essential to enable very high sensitivity measurement. However, fabrication of a subwavelength polarizer based on a metal grating with a high-aspect-ratio profile at the deep-subwavelength period level is difficult. In addition, direct combination of a WGP with surface plasmon resonance presents the problem of a narrow spectral band.

In this paper, a subwavelength polarizer with high extinction ratio in the broadband visible region is proposed by using the alternate metal and dielectric layers of a hyperbolic metamaterial (HMM) that is decorated on each side with a wire grid grating. This method is based on the fact that the HMM with its spatial frequency filtering characteristic enables the launch of high-spatial-spectrum bulk plasmon polariton modes [17–19] over a broad wavelength region, which thus supports the propagation of TM-polarized light in form of high-spatial-wavevector waves. In contrast, transverse electric (TE)-polarized light is almost completely absorbed inside the HMM. Numerical simulations indicate that extinction ratio of more than 50 dB could be realized throughout the visible region; in particular, the extinction ratio exceeds 80 dB within the wavelength region from 500 nm to 800 nm. This method indicates a potential way to perform high-sensitivity polarimetric imaging and detection.

Optics EXPRESS

2. Structure and principle

The configuration illustrated schematically in Fig. 1 is used to obtain a high-extinction-ratio subwavelength polarizer for operation in the broad visible wavelength range. The visible light impinges on the upper Al wire grid grating, which has 170 nm period and 0.5 duty cycle. Because the upper grating simply serves as a high-spatial-frequency exciter, groove depth of 40 nm is selected. The subwavelength grating enables generation of high-spatial-frequency spectrum diffraction waves with the transverse wavevector $k_x = \sqrt{\varepsilon_{Air}}\sin(\theta)k_0 + mk_g$, where ε_{Air} is the permittivity of the air surrounding the incident light; θ is the incident angle of light; $k_0 = 2\pi/\lambda_0$ is the wavevector of the incident light with wavelength λ_0 in vacuum; m is the diffraction order; and $k_g = 2\pi/p$ is the wavevector of the grating with period p. The HMM, which is composed of 10 alternately-stacked pairs of Ag/SiO_2 films (where each layer is 15 nm thick) is located beneath the upper grating. The HMM acts to block the transmission of any polarization-free light that impinges directly on its surface at any angle, but it allows the internal propagation of grating-coupled modes with TM-polarized spatial frequencies that are included within a specified band of values that all exceed the magnitude of the free-space wavevector k_0 significantly. Adjacent to the output side of the HMM is a lower wire grid grating, which enables conversion of the high-spatial-frequency waves that are coupled out of the HMM into a single-spatial-frequency plane wave that would propagate loss-free in the atmospheric environment. The lower grating has the same period, groove depth, and parallel groove direction as the upper grating. Additionally, the alignment or half of period shift between the upper and lower gratings would be required.

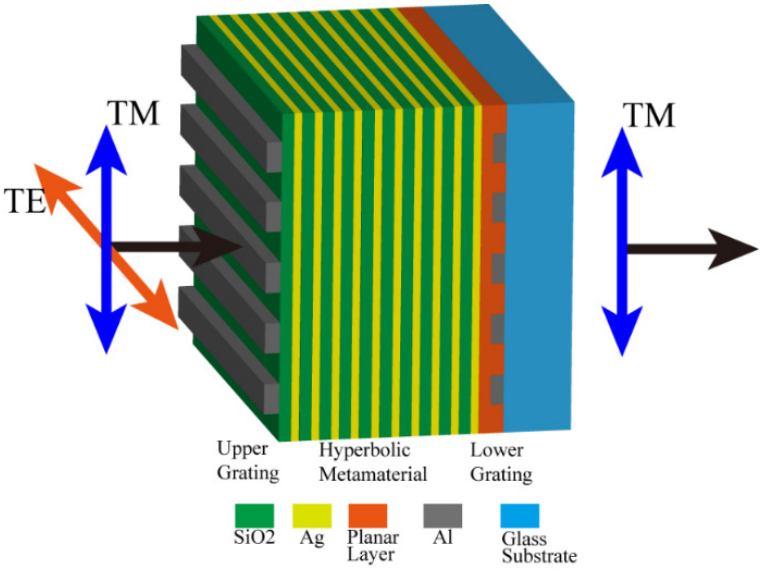

Fig. 1. Schematic of proposed subwavelength polarizer with high extinction ratio in the broadband visible region.

Given the fabrication feasibility of the designed structure, the prospective procedures are exhibited in the Fig. 2(a). This lower grating with low-aspect-ratio pattern would firstly be fabricated on the glass substrate by UV interference lithography in combination with ion beam etching. The PMMA (polymethyl methacrylate) or adhesive is used to planarize the lower grating and is cured using pressure or an I-line mercury lamp. The residual PMMA or adhesive acting as a spacer layer is reactive ion beam etched to obtain a planar profile with a remaining thickness of about 15 nm for further process. Subsequently, the HMM is implemented by alternately depositing the Ag and SiO_2 films on the planar layer. Fortunately,

Optics EXPRESS

the upper grating could be produced by UV exposure lithography and lift-off method to realize half of period shift with the lower grating. A sacrificial PMMA layer and photoresist is spun on the surface of HMM, which experiences the UV light illumination from the side of the lower grating. The electric intensity distribution inside the photoresist is shown in Fig. 2(b), which indicates that the exposure part of photoresist is aligned with the pattern of the lower grating. The reactive ion beam etching and lift-off process would be applied to transfer the photoresist pattern to be the Al grating pattern as shown in Fig. 2(a), which achieves half of grating period shift between the upper and lower gratings. For the simulation process, the permittivities of Al and SiO_2 were taken from the datasheets in [20] and that of Ag originated from the datasheets in [21]. The permittivities of the glass substrate, PMMA [22], and Photoresist [22] were set as 2.14, 2.3, and 2.59, respectively.

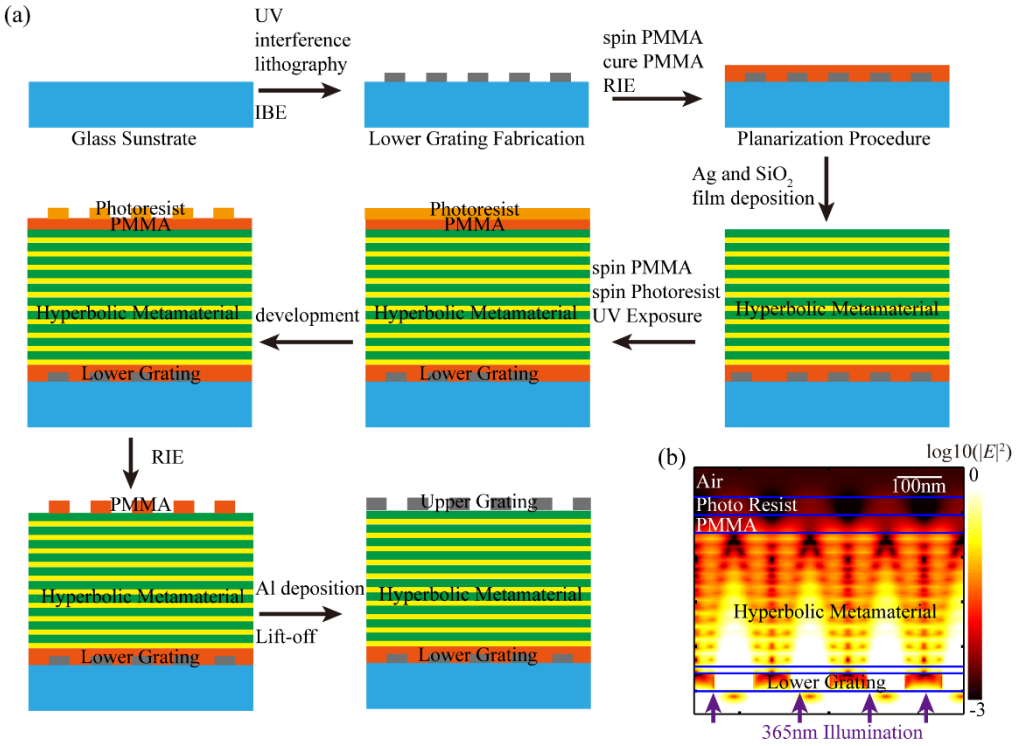

Fig. 2. (a) Schematic diagrams for the prospective processes of structure fabrication. (b) Cross-section of electric field intensity for the structure of lower grating incorporating HMM under the 365nm illumination in the process of fabricating the upper grating. The color bar is on logarithmic scale.

The HMM with metal-dielectric structures engineered on a deep-subwavelength scale materials enables offering an efficient way to manipulate the propagation of light to yield a number of novel and exotic phenomena. Figure 3 illustrates the relationship between the longitudinal wavevector k_z and the tangential wavevector k_x as calculated using the Bloch theorem, which clarifies the dispersion relationship of the multilayer-based HMM structure. When the light polarization state is that of TE wave, the HMM has a dispersion relationship similar to that of a homogeneous high-loss electromagnetic medium, as shown in Fig. 3(a). The real part of k_z is nearly zero and the imaginary part increases with the spatial wavevector in the visible region, which indicates that the TE-polarized light is evanescent inside the HMM and decays exponentially along the incident direction. This phenomenon means that the HMM could hamper the transmission of the TE diffraction wave by causing high absorption.

Optics EXPRESS

For TM-polarized incident light, the HMM based on the Ag/SiO_2 multilayer structure behaves like a homogeneous electromagnetic medium with highly anisotropic, hyperbolic spatial frequency dispersion [18]. Mutual coupling of the surface plasmon polariton between the adjacent metal-dielectric layers enables squeezing of the bulk plasmon polariton inside the HMM, which has a broad frequency response characteristic and a high spatial wavevector coupling capability. The plot of the real part of k_z versus variant k_x shown in Fig. 3(b) exhibits a hyperbolic profile with no cut-off spatial frequency, which indicates that evanescent waves with infinitely large wavevectors could be launched by the HMM when the light absorption is ignored. However, because of the quick growth of the imaginary part of k_z, ultrahigh spatial frequencies could not be supported, which means that the light modes within a specified k_x range of spatial frequencies would pass through the multilayer-based HMM.

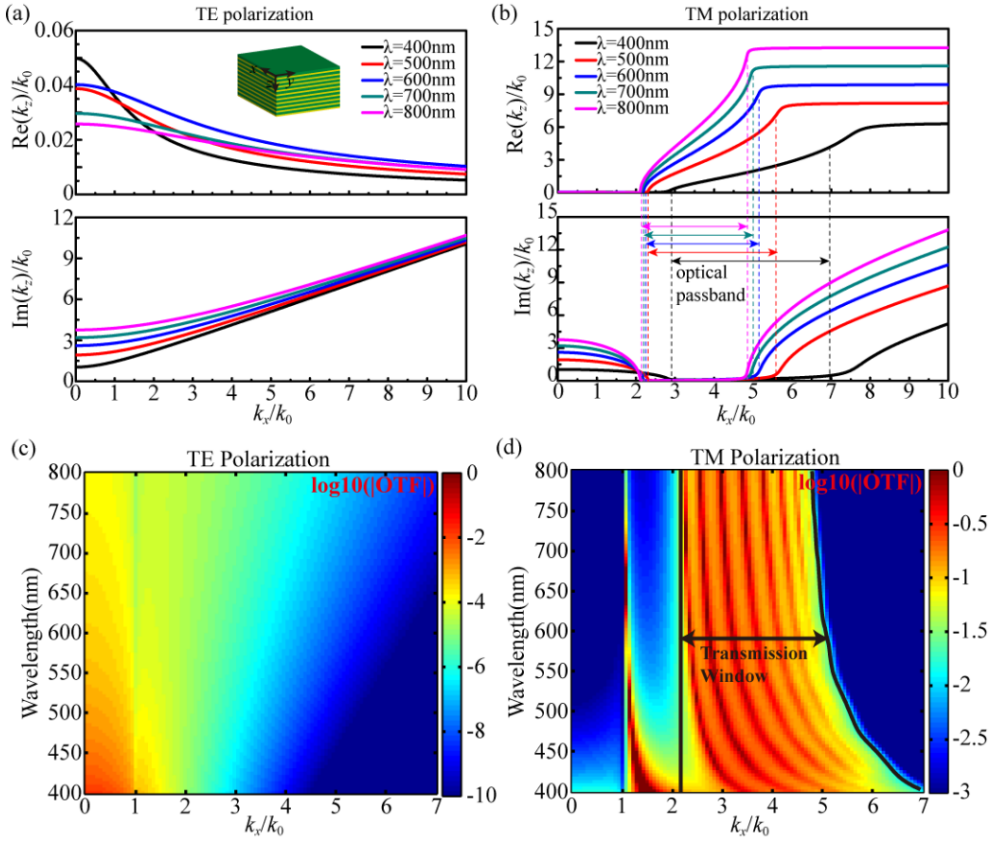

Fig. 3. Calculated real and imaginary parts of the longitudinal wavevector k_z versus variant tangential wavevector k_x in the proposed Ag/SiO_2 multilayer-based hyperbolic metamaterial (HMM) at incident light wavelengths of 400 nm, 500 nm, 600 nm, 700 nm, 800 nm for (a) TE-polarized and (b) TM-polarized light. The inset in (a) shows the proposed HMM. The optical transmission function (OTF) distributions of the multilayer-based HMM structure on a logarithmic scale as a function of the normalized transverse wavevector k_x/k_0 and the free space wavelength λ_0 are shown for (c) TE-polarized and (d) TM-polarized light illumination.

As expected, the calculated optical transmission function (OTF) for the proposed multilayer-based HMM structure exhibits damping behavior for any wavevectors with TE polarization and a transmission ability for specific wavevectors with TM polarization, as illustrated in Fig. 3(c) and 3(d), respectively. The OTF is calculated via the transfer matrix method [23] and is plotted in the positive half of the k-space. In Fig. 3(c), because of the high absorption inside the HMM for TE waves, all the spatial wavevectors show poor transmission

Optics EXPRESS

capabilities. The magnitude of the OTF is less than the order of −4 for the lower spatial frequency wavevectors and it rapidly declines to the order of −10 as the spatial wavevectors increase, which can be effectively ignored at the output port of the HMM. When compared with Fig. 3(c), Fig. 3(d) clearly shows that a low-absorption transmission window for the specific high-spatial-wavevector waves is created through the multilayer-based HMM under TM-polarized illumination at all the considered values of λ_0, which means that the diffracted waves from the upper grating with specific wavevectors could be coupled out of the HMM, while the other diffraction waves outside the specified window range are damped. At the position where $k_x = k_0$, the high transmission efficiency is mainly caused by the interaction of the modes at the interface between the input space and the HMM medium.

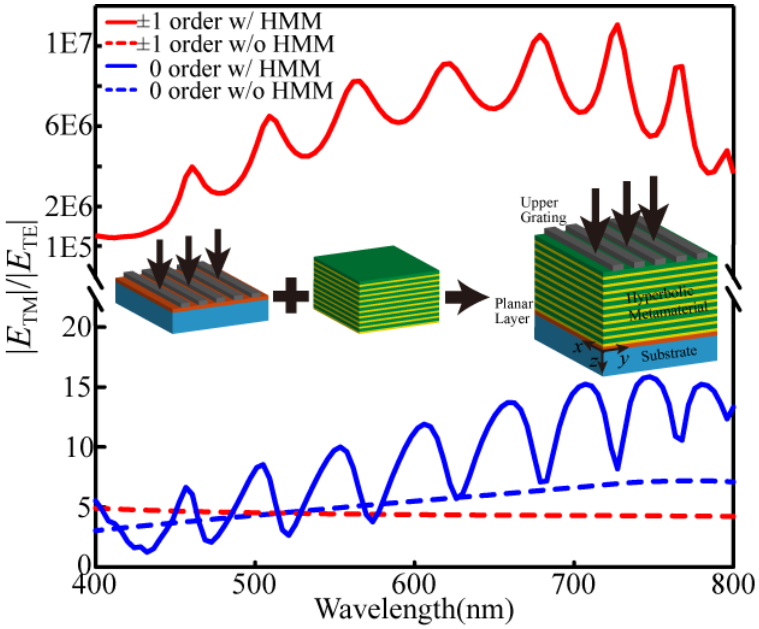

Fig. 4. Transmission amplitude ratio for the TM polarization and the TE polarization for the zeroth and ± 1st orders of the light diffracted from the upper grating with or without the HMM. The inset shows the structure of the upper grating when combined with the HMM on a glass substrate. The parameters are same as those used in Fig. 1.

The calculation is implemented using rigorous coupled wave theory [24], with results as shown in Fig. 4, to confirm that the HMM could inhibit TE waves remarkably while delivering TM waves, particularly for high-spatial-frequency wavevectors. For an upper grating with 170 nm period under normal incidence, the amplitude of the diffracted light with TM polarization is five-fold larger than that of the TE-polarized light for the zeroth and ± 1st order waves, as indicated by the dashed lines in Fig. 4. This trend is consistent with that of subwavelength wire grid grating serving as the polarizer. In addition, a grating with deeper grooves would exhibit a higher diffraction amplitude ratio for the TM polarization and the TE polarization, but this would also lead to high fabrication complex and would be difficult to implement using current fabrication capabilities.

However, this problem could be circumvented by incorporating multilayers-structure HMM with subwavelength wire grid grating as sketched in inset of Fig. 4. When the designed HMM is introduced to the wire grid grating, the spatial wavevector filtering behavior of the HMM under TM polarization would mean that the wavevectors of ± 1st order diffraction waves from the grating would fall into the filtering transmission window, and the TM-polarized light would propagate through the HMM in the form of high-spatial-frequency waves. The red solid line in Fig. 4 indicates that the transmission ability for TM waves is six

Optics EXPRESS

orders of magnitude greater than that for TE-polarized waves (red dashed line) over the broad visible wavelength range. For zeroth-order wave from the grating passing through the HMM structure, the blue solid line in Fig. 4 indicates that the transmission ratio of TM-polarized to TE-polarized light is approximately the same as that in the case without the HMM (blue dashed line). This phenomenon is attributed to the equal magnitude of the imaginary part of k_z in the dispersion curve as shown in Fig. 3(a) and 3(b), leading to the same absorption for the low-spatial-frequency wavevectors of the TE-polarized and TM-polarized waves. Therefore, it is important to realize high-extinction-ratio performance by engineering the transmission window of the HMM appropriately under TM polarization condition.

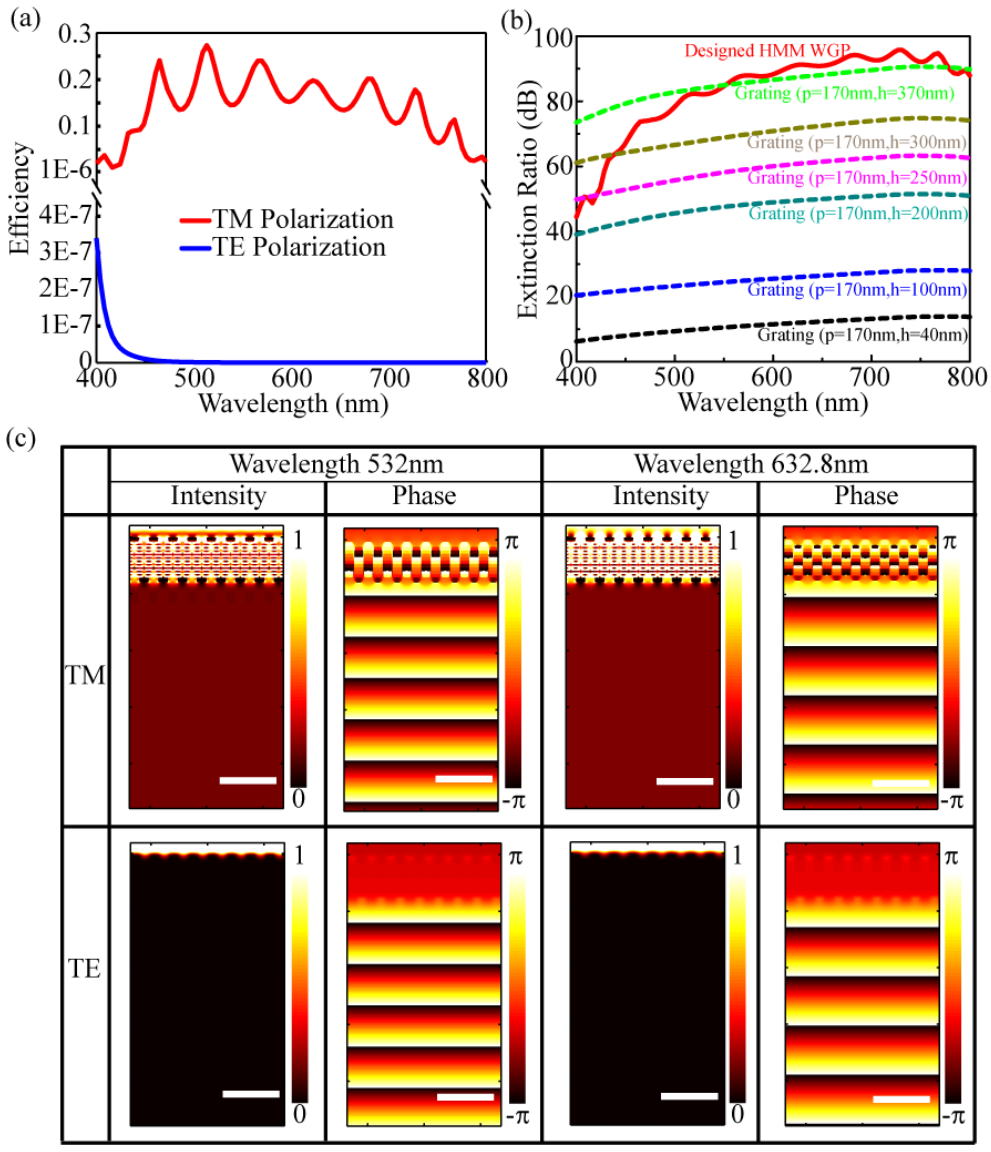

Fig. 5. (a) Transmission efficiency of TM-polarized (red line) and TE-polarized (blue line) incident light and (b) extinction ratio as a function of incident wavelengths. The solid line represents the results for the designed structure; dashed lines show the results for the Al wire grid grating with period p = 170 nm and various values of groove depth h. (c) Intensity and phase distribution at the wavelengths of 532 nm and 632.8 nm under TM-polarized and TE-polarized light conditions. The scale bars represent 500 nm.

Optics EXPRESS

3. Results and discussion

Calculations for the simulations of the proposed configuration were performed using COMSOL software to give the results shown in Fig. 5, which shows the transmission efficiency and extinction ratio characteristics of the designed subwavelength polarizer over the wavelength range from 400 nm to 800 nm. For TE-polarized wave, as shown in Fig. 5(a), the transmission efficiency over the entire visible wave range is low and could almost be ignored. However, for TM-polarized wave, the transmission efficiency in the visible region is approximately 0.15 in the 450 to 730 nm wavelength region, which is much greater than that for TE-polarized wave. The transmission efficiency at the edge of the wavelength range is relatively low because the wavevectors of the ± 1st order diffraction waves lay at the edge of the transmission window with nonzero absorption of the imaginary part of k_z in the dispersion relation. In addition, the transmission efficiency curve for the TM polarization shows a tendency to fluctuate. This phenomenon could undoubtedly be relieved by expanding the transmission window of the HMM.

In Fig. 5(b), the red solid line represents the extinction ratio of the designed structure, which exceeds 50 dB over the entire visible wavelength region and is particularly high over the wavelength region from 500 nm to 800 nm, where the extinction ratio reaches more than 80 dB. In addition, we also calculated the extinction ratio of a conventional Al wire grid grating with period p = 170 nm and different groove depths. It is clear that the extinction ratio of the conventional Al wire grid grating could be improved by increasing the groove depth of the grating, but the extent to which the extinction ratio could be increased is finite because of the limitation of fabrication difficulty and complexity. When the extinction ratio of conventional Al wire grid grating can be matched with that of the designed structure, the aspect ratio of Al grating is required to reach 4.35 for the period p = 170nm.

Figure 5(c) presents the electric field intensity and phase distribution for the subwavelength polarizer under TE and TM polarization conditions at the operating wavelengths of 532 nm and 632.8 nm. The phase distribution shows that the single-spatial-wavevector plane wave propagates along the z direction without any stray wavevectors at the output port of the proposed structure. The electric field intensity distribution at the output plane of the structure also confirms that the transmission magnitude for the TM polarization surpasses that for the TE polarization quite remarkably.

For the proposed method, the filtering transmission window of the HMM under TM polarization conditions is the primary determination of the polarimetric performance, so the extinction ratio of the subwavelength polarizer could be modulated by varying the parameters of the HMM's component materials. The OTF distribution of the multilayer-based HMM versus the normalized transverse wavevector k_x/k_0 and the thickness of the SiO_2 layer is calculated in Fig. 6(a). The result in Fig. 6(a) shows that decreasing the thickness of the SiO_2 layer could push the center wavevector of the filtering window towards a higher spatial frequency with a wider spatial wavevector transmission region. However, the shift of the filtering transmission window leads that the upper-grating-coupled modes for the different wavelength is outside the transmission window, which would suppress the transmission efficiency of TM-polarized light at the edge of the wavelength range, as shown in Fig. 6(c). On the other hand, the same simulation are preformed to calculate the OTF distribution as a function of the thickness of the Ag layer in Fig. 6(b). Decreasing the thickness of the Ag layer could hold the center wavevector of the filtering window with a wider spatial wavevector region, which is a way to improve the transmission efficiency of TM-polarized light for the subwavelength polarizer in the broad wavelength region, as shown in Fig. 6(d). However, thinner metal layer gives rise to a more difficult fabrication process. Figure 6(e) and 6(f) are the distribution of extinction ratio for the subwavelength polarizer as a function of the thickness of the SiO_2 and Ag layer, which exhibits the magnitude of extinction ratio at the region of long wavelength could be increased by decreasing the thickness of HMM's

Optics EXPRESS

component materials. The phenomenon is attributed to the wide spatial wavevector transmission region for TM-polarized light.

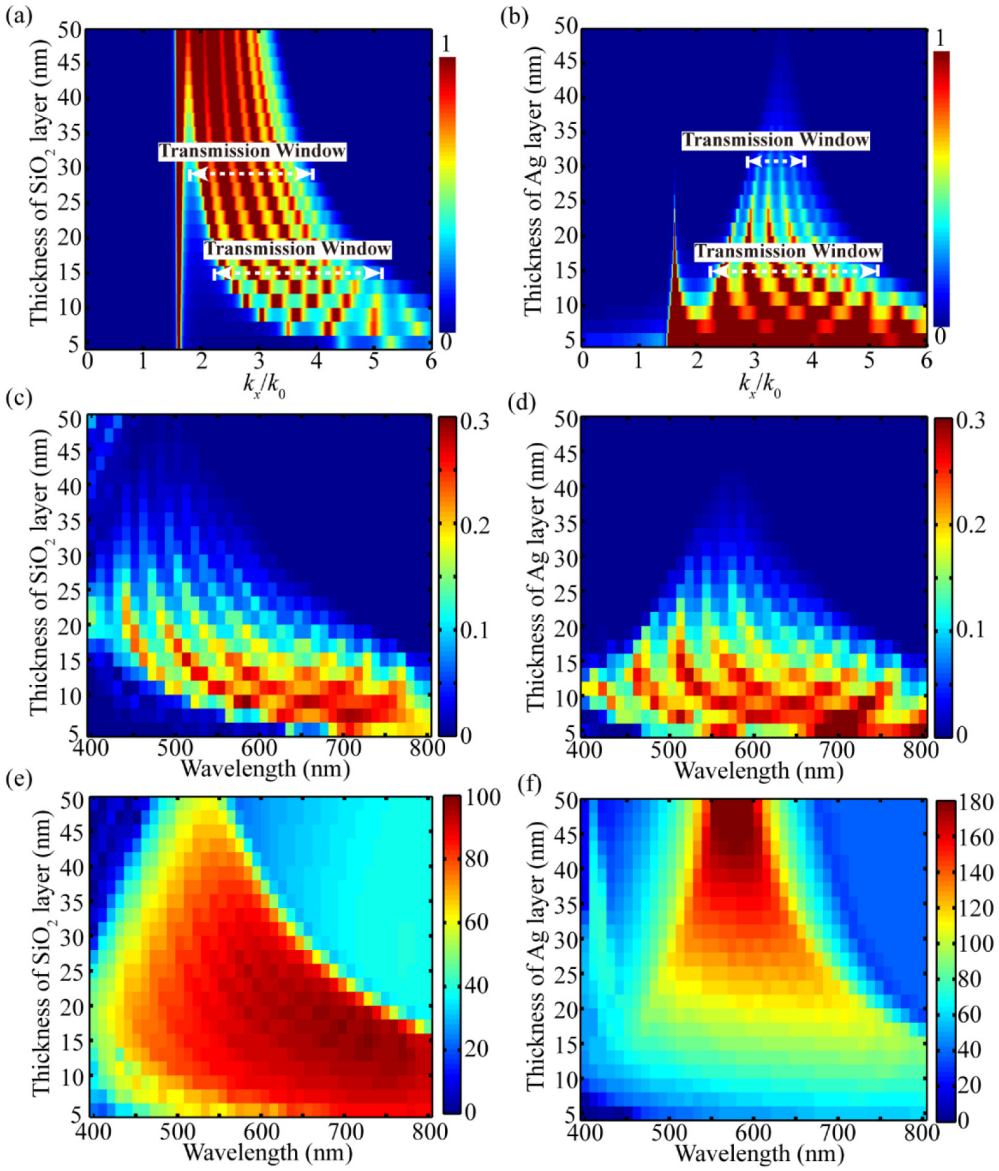

Fig. 6. (a) Calculated OTF distributions versus the normalized transverse wavevector k_x/k_0 and the thickness of the SiO_2 layer in the multilayer structure. (b) OTF distribution for variant thickness of the Ag layer. When tuning the thickness, other parameters are kept unchanged. The illumination wavelength is 532nm. (c) Transmission efficiency of TM-polarized light and (e) extinction ratio of the proposed subwavelength polarizer as a function of the thickness of the SiO_2 layer and the wavelength. (d)Transmission efficiency of TM-polarized light and (f) extinction ratio of the proposed subwavelength polarizer for variant thickness of the Ag layer. The magnitude of the extinction ratio is on the decibel scale.

More layers in the HMM will mean increased incident light absorbability, but the loss effect will be much more acute for the TE polarization than for the TM polarization light, as indicated by the analysis of the dispersion relation (Fig. 3). Therefore, the extinction ratio

Optics EXPRESS

could be improved remarkably by increasing the number of pairs of the HMM's component layers, as shown in Fig. 7(a).

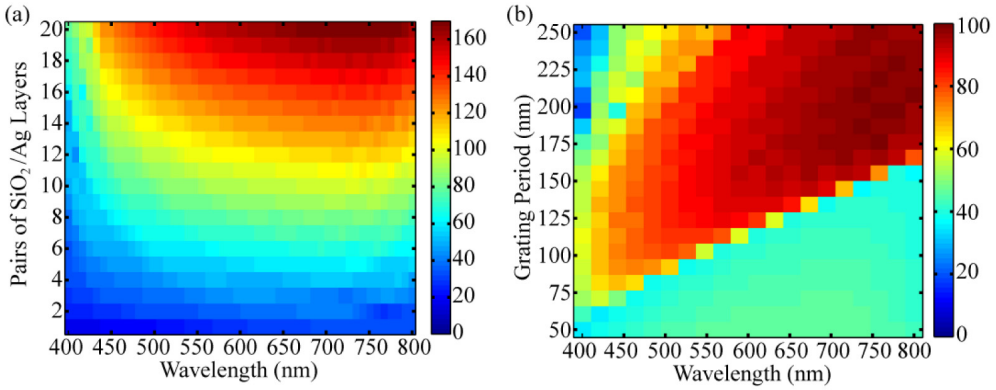

Fig. 7. (a) Extinction ratio of the designed structure as a function of the number of pairs of SiO_2/Ag layers and the wavelength. (b) Extinction ratio as a function of the grating period and wavelength. The magnitude of the extinction ratio is on the decibel scale.

In addition, tuning of the period of the grating is also anticipated to allow the peak of the extinction ratio to be varied over the incident light wavelength region. As shown in Fig. 7(b), the extinction ratio would be enhanced at shorter wavelengths as the grating period gradually shrinks; this is attributed to the fact that the 1st order diffraction wave from the grating for shorter wavelengths is near the center position of the filtering transmission window rather than the edge. The peak position of the extinction ratio over the wavelength region of interest is thus determined by the grating period and the filtering transmission window of the HMM. Generally speaking, it is more feasible to tune the incident wavelength band by varying the parameters of the HMM, which would be much easier than small period grating fabrication.

4. Conclusion

In summary, a high-extinction-ratio and broadband visible subwavelength polarizer is achieved using an alternating metal and dielectric layer-based HMM sandwiched between upper and lower subwavelength Al wire grid gratings. Simulation results show that the extinction ratio of the designed subwavelength polarizer would exceed 50 dB over the whole visible wavelength region from 400 nm to 800 nm and would reach a maximum magnitude of 95 dB at a wavelength of 725 nm, which would be equivalent to a conventional Al grating-based WGP with an aspect ratio of 4.35 at the deep subwavelength period level. The proposed method thus exhibits a more realizable fabrication process than that used for a conventional WGP for high-extinction-ratio performance. In addition, the scheme enables the production of a polarizer with a higher extinction ratio and a variable wavelength region by tuning the permittivities and thicknesses of the components of the multilayer structure. It is believed that the subwavelength polarizer in this work has great potential for use in the high-sensitivity charge-coupled device (CCD) polarimetric imaging, detection and display fields.

Funding

National Key R&D Program of China (No. 2018YFF01011000); National Natural Science Foundation of China (NSFC) (61605197, 61805233).

Acknowledgments

We thank the National engineering research center for diffraction gratings manufacturing and application of China.

Optics EXPRESS

References

1. M. Alouini, F. Goudail, A. Grisard, J. Bourderionnet, D. Dolfi, A. Bénière, I. Baarstad, T. Løke, P. Kaspersen, X. Normandin, and G. Berginc, "Near-infrared active polarimetric and multispectral laboratory demonstrator for target detection," Appl. Opt. **48**(8), 1610–1618 (2009).
2. F. Snik, J. C. Jones, M. Escuti, S. Fineschi, D. Harrington, A. D. Martino, D. Mawet, J. Riedi, and J. S. Tyo, "An overview of polarimetric sensing techniques and technology with applications to different research fields," Proc. SPIE **9099**, 90990B (2014).
3. D. K. Beamer, U. Abeywickrema, and P. Banerjee, "Polarization vector signatures for target identification," Proc. SPIE **10407**, 104070T (2017).
4. G. R. Bird and M. Parrish, "The wire grid as a near-infrared polarizer," J. Opt. Soc. Am. **50**(9), 886–891 (1960).
5. H. Tamada, T. Doumuki, T. Yamaguchi, and S. Matsumoto, "Al wire-grid polarizer using the s-polarization resonance effect at the 0.8-microm-wavelength band," Opt. Lett. **22**(6), 419–421 (1997).
6. S. W. Ahn, K. D. Lee, J. S. Kim, S. H. Kim, J. D. Park, S. H. Lee, and P. W. Yoon, "Fabrication of a 50 nm half-pitch wire grid polarizer using nanoimprint lithography," Nanotechnology **16**(9), 1874–1877 (2005).
7. Z. Yu, P. Deshpande, W. Wu, J. Wang, and S. Y. Chou, "Reflective polarizer based on a stacked double-layer subwavelength metal grating structure fabricated using nanoimprint lithography," Appl. Phys. Lett. **77**(7), 927–929 (2000).
8. J. J. Wang, L. Chen, X. Liu, P. Sciortino, F. Liu, F. Walters, and X. Deng, "30-nm-wide aluminum nanowire grid for ultrahigh contrast and transmittance polarizers made by UV-nanoimprint lithography," Appl. Phys. Lett. **89**(14), 141105 (2006).
9. Y. Ekinci, H. H. Solak, C. David, and H. Sigg, "Bilayer Al wire-grids as broadband and high-performance polarizers," Opt. Express **14**(6), 2323–2334 (2006).
10. F. Meng, J. Chu, Z. Han, and K. Zhao, "The design of the sub-wavelength wire-grid polarizer," in Proceedings of the 7th IEEE International Conference on Nanotechnology (IEEE, 2007), pp. 942–946.
11. J. J. Wang, F. Walters, X. Liu, P. Sciortino, and X. Deng, "High-performance, large area, deep ultraviolet to infrared polarizers based on 40 nm line/78 nm space nanowire grids," Appl. Phys. Lett. **90**(6), 061104 (2007).
12. L. J. Guo, "Recent progress in nanoimprint technology and its applications," J. Phys. D Appl. Phys. **37**(11), R123–R141 (2004).
13. R. Wang, T. Li, X. Shao, X. Li, X. Huang, J. Shao, Y. Chen, and H. Gong, "Subwavelength gold grating as polarizers integrated with InP-based InGaAs sensors," ACS Appl. Mater. Interfaces **7**(26), 14471–14476 (2015).
14. D. Sun, T. Li, B. Yang, X. Shao, X. Li, and Y. Chen, "Research on polarization performance of InGaAs focal plane array integrated with superpixel-structured subwavelength grating," Opt. Express **27**(7), 9447–9458 (2019).
15. J. J. Peltzer, P. D. Flammer, T. E. Furtak, R. T. Collins, and R. E. Hollingsworth, "Ultra-high extinction ratio micropolarizers using plasmonic lenses," Opt. Express **19**(19), 18072–18079 (2011).
16. C. Lee, E. Sim, and D. Kim, "Blazed wire-grid polarizer for plasmon-enhanced polarization extinction: design and analysis," Opt. Express **25**(7), 8098–8107 (2017).
17. Y. Xiong, Z. Liu, C. Sun, and X. Zhang, "Two-dimensional imaging by far-field superlens at visible wavelengths," Nano Lett. **7**(11), 3360–3365 (2007).
18. T. Xu and H. J. Lezec, "Visible-frequency asymmetric transmission devices incorporating a hyperbolic metamaterial," Nat. Commun. **5**(1), 4141 (2014).
19. W. Kong, W. Du, K. Liu, C. Wang, L. Liu, Z. Zhao, and X. Luo, "Launching deep subwavelength bulk plasmon polaritons through hyperbolic metamaterials for surface imaging with a tuneable ultra-short illumination depth," Nanoscale **8**(38), 17030–17038 (2016).
20. E. D. Palik, *The handbook of optical constants of solids* (Academic 1985)
21. P. B. Johnson and R. W. Christy, "Optical constants of the noble metals," Phys. Rev. B **6**(12), 4370–4379 (1972).
22. N. Fang, H. Lee, C. Sun, and X. Zhang, "Sub-diffraction-limited optical imaging with a silver superlens," Science **308**(5721), 534–537 (2005).
23. M. Born and E. Wolf, *Principles of optics* (Elsevier 2013).
24. M. G. Moharam, E. B. Grann, D. A. Pommet, and T. K. Gaylord, "Formulation for stable and efficient implementation of the rigorous coupled-wave analysis of binary gratings," J. Opt. Soc. Am. A **12**(5), 1068–1076 (1995).